Tetrahedron 66 (2010) 9694–9702

Contents lists available at ScienceDirect

Tetrahedron

journal homepage: www.elsevier.com/locate/tet

Synthesis and characterisation of medium-sized ring systems by oxidative cleavage. Part 2: Insights from the study of ring expanded analogues

Tomas Lebl *, Magali M. Lorion, Alan M. Jones, Douglas Philp, Nicholas J. Westwood *

School of Chemistry and Biomedical Sciences Research Complex, University of St Andrews, St Andrews, Fife KY16 9ST, Scotland, UK

ARTICLE INFO

Article history:
Received 13 July 2010
Received in revised form 28 September 2010
Accepted 18 October 2010
Available online 11 November 2010

Keywords:
Heterocycle
Oxidative fragmentation
Medium-sized ring
VT NMR analysis
Mechanism

ABSTRACT

Variable temperature NMR analysis and computational methods have been used to develop a detailed understanding of the ^{1}H NMR spectra of a family of medium-sized ring containing compounds. The family consists of analogues containing 10-, 11- and 12-membered rings and in all cases the NMR spectra at room temperature showed a series of diastereotopic methylene signals despite the lack of a stereogenic centre in these systems. On repeating the NMR analysis at higher temperatures, all the signals coalesced for the 12-membered ring system consistent with full interconversion of ring conformers. This was not observed in the analogous 10- and 11-membered ring systems with the interchange of conformers remaining slow on the NMR timescale. However, 1D gs-NOESY/EXSY NMR experiments showed that in the smaller ring systems interconversion of diastereotopic protons did occur. Computational studies suggest that the dynamic process observed by NMR for the 10- and 11-membered rings systems is different from that observed in the 12-membered ring containing compound.

1. Introduction

There remains significant interest in the search for chemical scaffolds that exhibit restricted conformational freedom and hence display functional groups in well-defined orientations.[1] Medium-sized ring systems are considered useful in this context due to the often strong conformational preferences they exhibit.[2,3] Importantly, very few examples of medium-sized ring containing compounds are present in the commercial compound collections that dominate many high-throughput screening programmes. For this reason and others, synthetic routes to access medium-sized rings are of continued importance. To date, our focus has been on the use of oxidative fragmentation reactions as a means of accessing these types of systems.

In the previous paper,[4] we revisited the synthesis of the medium-sized ring containing compound **1a** by oxidative fragmentation of the known anti-psoriasis drug **2a** (Fig. 1A).[5] Compound **1a** had a relatively complex ^{1}H NMR spectrum containing a series of diastereotopic protons associated with the methylene groups present in the 10-membered ring. This observation implied that **1a** contains at least one non-classical stereogenic axis. One possible explanation was that this stereogenic axis resulted from restricted rotation about the N12–C1′-bond in **1a** and whilst this clearly makes a contribution to the complexity of the ^{1}H NMR spectrum of **1a** at room temperature, variable temperature NMR studies showed that the situation is more complex as the C7–C10 protons remained diastereotopic at temperatures well above that required for coalescence of the aromatic signals in **1a**. In addition, the small molecule X-ray crystal structure of **1a** showed that in the unit cell four different conformers were represented.[6] Two of these structures ((i) and (ii), Fig. 1B) are non-superimposable mirror images. The other two ((iii) and (iv)) correspond to a second enantiomeric pair in which the chlorine atom is on the opposite face of the molecule relative to (i) and (ii), respectively. The relative orientation of the three carbonyl groups is the same in all four conformers.

Whilst the observation of restricted bond rotation in medium-sized ring systems is relatively common,[2,7] we became interested in exploring this system further as a function of ring size. The results of these studies are presented here including a detailed discussion of variations in the ability of the amide group to reorient itself as the size of the ring varies.

2. Results and discussion

Our previously reported[4] variable temperature NMR studies on **1a** showed a considerable broadening of the two signals associated with the diastereotopic C7 protons as a function of temperature (Fig. 2(a) and (b), Fig. 1A for numbering and Ref. 4). Broadening of these resonances at higher temperatures is probably consistent with a relaxation of restrictions to bond rotation in the 10-membered ring of

* Corresponding authors. E-mail addresses: tl21@st-andrews.ac.uk (T. Lebl), njw3@st-andrews.ac.uk (N.J. Westwood).

0040-4020/$ – see front matter © 2010 Elsevier Ltd. All rights reserved.
doi:10.1016/j.tet.2010.10.043

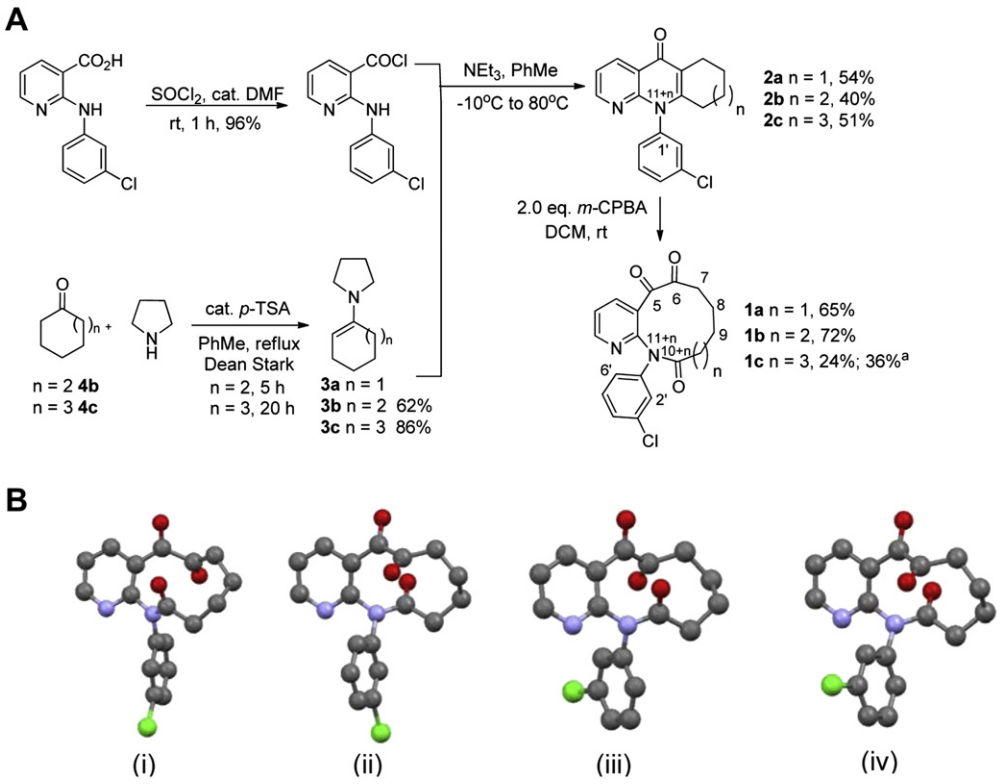

Fig. 1. A. Synthesis of the medium-sized ring containing compounds **1a**–**c**. [a]A small increase in yield was observed when 4.0 equiv of *m*-CPBA was used. B. The four independent conformers that make up the unit cell in the X-ray crystal structure analysis of **1a**.

1a. In order to characterise this further, it was decided to repeat the NMR analysis on analogues of **1a** that contained larger ring systems (11- or 12-membered ring in **1b** and **1c**, respectively, Fig. 1A).

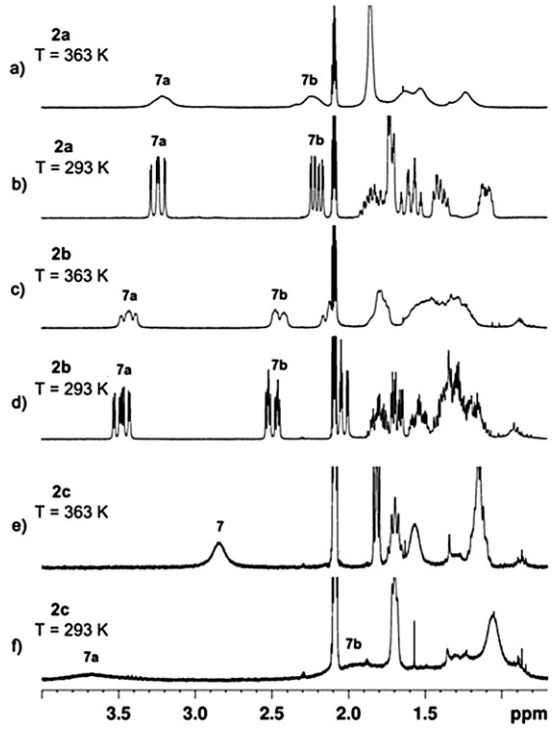

Fig. 2. Comparison of the aliphatic region of the ^{1}H NMR (300 MHz) spectra for **1a**, **1b** and **1c** recorded in toluene-d_8 at 293 and 363 K showing broadening or coalescence of the C7-diastereotopic proton resonances.

2.1. Synthesis of ring expanded analogues of 1a

The required analogues **1b** and **1c** were synthesised in an analogous manner to **1a** (Fig. 1A). The enamines **3b** and **3c** were prepared according to a literature procedure from cycloheptanone (**4b**) and cyclooctanone (**4c**), respectively, and were converted to the desired pyridones **2b** and **2c**.[8] Oxidative cleavage of **2b** and **2c** was achieved on reaction with *m*-CPBA, with the 11-membered macrocycle **1b** being afforded in a similar yield (72%) to that obtained for the 10-membered macrocycle **1a** (65%). However, synthesis of the 12-membered ring macrocycle **1c** proved much more difficult, apparently due to an overall decrease in the reactivity of **2c** with *m*-CPBA. When 2 equiv of *m*-CPBA was used, **1c** was isolated in 24% yield and a second product was obtained in 30% yield. ^{1}H NMR analysis indicated that this new product contained an aldehyde functional group. Further NMR studies led to the assignment of this product as **5** and a plausible mechanism for formation of **5** from **2c** is shown in Scheme 1. It seems likely that when n=1 (**2a**) the corresponding iminium ion **6** is rapidly intercepted by a second equivalent of *m*-CPBA to give **7** (probably as a single *syn*-diastereomer[9]). However, if in the case of the eight-membered ring, this attack is slowed due to increased steric hindrance to attack of the nucleophile, conversion of iminium ion **8** to enamine **9** may compete. Subsequent oxidative cleavage of the enamine double bond can then occur to give **5**. A small increase in the yield of **1c** from **2c** was observed when 4 equiv of *m*-CPBA was used.

In Part 1,[4] it was shown that whilst it was possible to prepare **1a** from **2a** in a catalytic ruthenium tetroxide-mediated oxidative cleavage reaction, the major product formed in this reaction was often the *syn*-diol **10** (Scheme 1). Under conditions that gave only **10** from **2a**, it was found that **2c** was converted to **1c** in 16% yield (73% based on recovered starting material **2c**) with no indication of the corresponding diol **11** being present. Whilst an increase in the catalyst loading to 5 mol %, resulted in an increase in the isolated

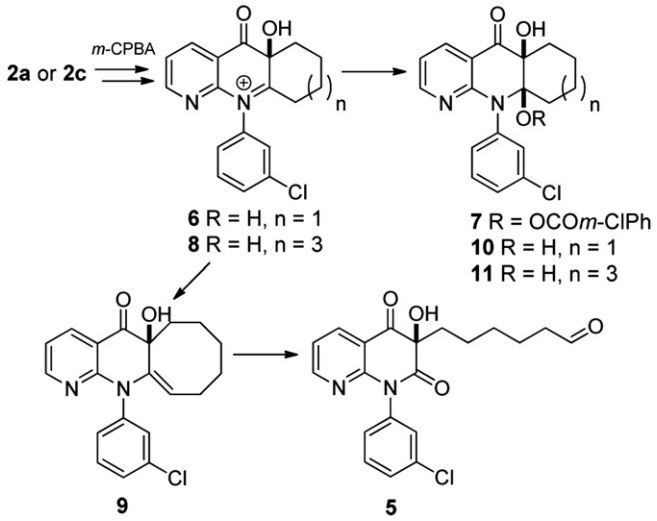

Scheme 1. A possible mechanism for the formation of **5**.

yield of **1c** to 37% isolated yield (66% based on recovered starting material **2c**), **11** was still not observed. The subtle difference in behaviour of **2a** and **2c** in this reaction is currently rationalised either based on differences in the rate of cleavage of the corresponding diols **10** and **11** by sodium periodate (which is used as a co-oxidant) or by a change in mechanism with, for example, direct cleavage[10] of the double bond in **2c** occurring.

2.2. Variable temperature NMR study of the 10, 11 and 12-membered ring containing systems, 1a–c

A comparison of the aliphatic region of the ^{1}H NMR spectra obtained for the three medium-sized ring systems in **1a**, **1b** and **1c** as a function of temperature is shown in Fig. 2.

The results at 293 K (Fig. 2(b), (d) and (f)) indicate that the dynamics of this system vary as a function of ring size with a significant transition taking place as the ring size is increased from 11 to 12 (cf. Fig. 2d and f). In **1c** (12-membered ring) the aliphatic signals are very broad with the signals assigned to the C7-diastereotopic protons (labelled 7a and 7b) being barely visible, whereas the analogous signals in **1b** (11-membered ring) are similar to those observed for **1a**. When the ^{1}H,^{13}C-HSQC spectrum of **1c** was recorded at lower temperature (233 K, see Fig. S1)[11] six sets of diastereotopic aliphatic protons were observed with the spectrum being further complicated by the presence of two rotamers (2:1 ratio) resulting from restricted rotation about the N(14)–C(1′) bond at this temperature (see Fig. 1A for numbering system). The largest and smallest differences in chemical shifts (1.97 and 0.16 ppm) were associated with the C7 and C12 diastereotopic protons, respectively. Therefore, a preliminary explanation for this observation was that the diastereotopic nature of these protons stems from restricted rotation about the C5–C6 carbon bond of the dicarbonyl functionality in **1c** (Fig. 1A). However, further assignment of the ^{13}C resonances of the other methylene carbons in **1c** using a ^{1}H,^{13}C-H2BC experiment revealed that the diastereotopic pair with the second largest chemical shift difference belonged to C11.[11] The situation was clearly more complex than the initial explanation. Therefore, further studies using NMR and computational methods were carried out and are described below. Interestingly, the chemical shift differences of the diastereotopic protons calculated for the ground state of **1c** at the B3LYP/6-31G** level of theory showed a reasonable agreement with the observed trend (Table 1) providing evidence that this level of theory is relevant to the study of these systems, as expected.

Table 1
Chemical shift differences of diastereotopic protons in ppm derived from ^{1}H,^{13}C-HSQC of **1c** at 233 K and calculated for the ground state of **1c** at the B3LYP/6-31G** level of theory

	Experimental	B3LYP/6-31G**
C7	1.97	1.51
C8	0.84	0.76
C9	0.21	0.66
C10	0.45	0.68
C11	1.16	0.88
C12	0.16	0.48

Raising the temperature at which the ^{1}H NMR analysis was carried out to 363 K further emphasised the difference in behaviour between the 10- and 11-membered systems, **1a** and **1b**, as compared to the 12-membered system, **1c**. In the case of **1c**, a ^{1}H,^{13}C-HSQC spectrum recorded at 363 K showed that the signals corresponding to all the diastereotopic protons in **1c** coalesced on heating the sample (see Figs. 2e and S2[11]). Therefore the dynamics of the 12-membered ring are such that full interconversion of conformers occurs. On the other hand, the signals in the aliphatic region of the spectrum of **1b** remained separate and broadened as previously described[4] for **1a** (Fig. 2c vs Fig. 2a).

Since broadening of lines in the NMR spectrum as a function of temperature did not allow for unambiguous conclusions to be made concerning the dynamics of the 10- and 11-membered ring compounds, **1a** and **1b**, further studies using a 1D gs-NOESY/EXSY experiment were carried out at various temperatures (Fig. 3). For both **1a** and **1b** qualitatively similar results were obtained. At room temperature antiphase peaks due to a positive NOE were observed (Fig. 3a for **1a**, data for **1b** not shown). However, at higher temperatures the resonances associated with H7a and H7b appeared in phase indicating that chemical exchange of those two diastereotopic protons was occurring (Fig. 3b). As expected, the intensity of the

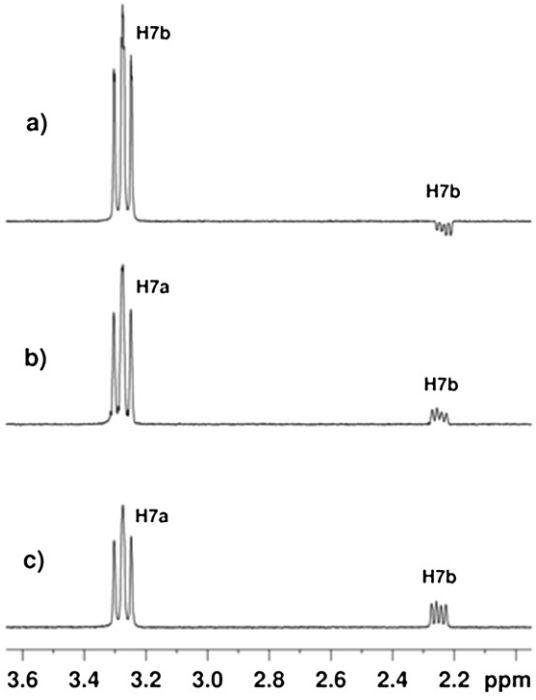

Fig. 3. 1D gs-NOESY/EXSY spectra recorded for **1a** following selective irradiation of the H7a resonance. (a) At 293 K the H7b peak has the opposite phase to the H7a peak as a result of a positive NOE (mixing time=0.4 s); (b) At 310 K the H7a and H7b peaks appear in the spectrum in phase because magnetisation transfer due to chemical exchange outweighs the NOE effect (mixing time=0.4 s); (c) At 314.5 K a faster rate of exchange and longer mixing time (0.5 s) results in a stronger enhancement of the H7b peak.

EXSY peaks proved to be dependent on both the temperature and the mixing time (Fig. 3c).

2.3. Rationalisation of the trends observed in the variable temperature NMR studies

The studies described above indicated that the dynamics of this system are very dependent on the size of the ring. The next step in providing a full rationalisation was to calculate the activation parameters for the dynamic processes associated with **1a**–**c** and to assess possible pathways to explain these using calculations at the B3LYP/6-31G** level of theory.

2.4. Restricted rotation about the N(12/13/14)–C(1′) bond in 1a, 1b and 1c

The activation parameters for restricted rotation about the N(13/14)–C(1′) bond in **1b** and **1c** were determined by total lineshape analysis of the C2′ and/or C6′ proton resonances and calculated at the B3LYP/6-31G** level of theory to be compared with the values already obtained for **1a** (Table 2).[4,11]

Table 2
Activation parameters $\Delta G^{\ddagger}_{298}$ [kJ mol^{-1}], $\Delta H^{\ddagger}$ [kJ mol^{-1}] and $\Delta S^{\ddagger}$ [kJ K^{-1} mol^{-1}] for restricted rotation about the N(12/13/14)–C(1′) bond determined experimentally using total lineshape analysis of ^{1}H NMR resonances of aromatic protons C2′ and/or C6′ and calculated at the B3LYP/6-31G** level of theory

	Experimental			B3LYP/6-31G**		
	$\Delta G^{\ddagger}_{298}$	$\Delta H^{\ddagger}$	$\Delta S^{\ddagger}$	$\Delta G^{\ddagger}_{298}$	$\Delta H^{\ddagger}$	$\Delta S^{\ddagger}$[a]
1a	55.6±0.1	56.1±0.7	1.7±2.8	60.8	61.0	0.8
1b	50.7±0.1	55.5±1.0	16.3±3.9	59.0	60.8	6.0
1c	51.9±0.9	54.8±1.4	9.6±5.8	55.7	54.3	−4.7

[a] All vibrational modes with frequencies below 300 cm^{-1} were ignored in calculating activation entropy.

The trend in the Gibbs free energy of activation ($\Delta G^{\ddagger}_{298}$) shows that the number of methylene groups has only a small effect on the restricted rotation about the N(12/13/14)–C(1′) bond (Table 2, column 2). The calculated values of activation enthalpy $\Delta H^{\ddagger}$ (Table 2, column 6) are in reasonably good agreement with the experimental values (Table 2, column 3), providing further support for the use of these computational methods in the context of this system. Surprisingly, however, the activation entropies for the restricted rotation about the N(12/13/14)–C(1′) bond ($\Delta S^{\ddagger}$, column 4) were all positive. One possible explanation for this comes from comparison of the calculated ground and transition state geometries of **1a**–**c** (Fig. S6 and Table S2).[11] When the transition states of **1a**–**c** are reached, the average increase in the N(12/13/14)–C(11/12/13) and N(12/13/14)–C(12a/13a/14a) bond lengths within the medium-sized ring was calculated to be 0.0150±0.0032 and 0.0185±0.003 Å, respectively. This may in turn result in a higher conformational flexibility of the ring and consequently to higher entropy. Unfortunately, a rather unsatisfactory agreement between experimental and theoretical data was obtained for the entropy of activation $\Delta S^{\ddagger}$ even when all vibrational entropy contributions from frequencies below 300 cm^{-1} were removed (cf. Table 2, column 4 vs column 7).

2.5. Dynamic processes associated with the medium-sized ring

2.5.1. Identification of the activation parameters. The resonances associated with the C7-diastereotopic protons in the ^{1}H NMR spectra of **1a**, **1b** and **1c** recorded between 278 and 373 K were subjected to total lineshape analysis. No interference caused by restricted rotation about the N(12/13/14)–C(1′) bond occurred as this process was already in the fast exchange limit in this temperature range. The resulting activation parameters $\Delta G^{\ddagger}_{298}$, $\Delta H^{\ddagger}_{298}$ and $\Delta S^{\ddagger}_{298}$ are presented in Table 3. In the case of **1a** and **1b**, the temperature range over which broadening of resonances was suitable for lineshape analysis was narrow and poor R^2 values resulted from the Eyring plots.[11] Therefore, quantitative EXSY spectra were also used for the calculation of the activation parameters. Very good agreement between the two methods was obtained for $\Delta H^{\ddagger}_{298}$ (Table 3, column 3 vs column 6) and whilst $\Delta S^{\ddagger}_{298}$ values showed considerable discrepancies, the errors resulting from the EXSY data were significantly smaller (Table 3, columns 4 and 7). All activation parameters clearly confirmed the difference in behaviour between the 12-membered system, **1c**, as compared to the 10- and 11-membered systems, **1a** and **1b**.

*2.5.2. Detailed assessment of **1c**.* With the experimentally determined activation parameters in hand, it was decided to investigate the dynamic processes associated with the medium-sized ring using computational techniques. As a starting point, it was assumed that the dynamic process being observed in the ^{1}H VT NMR experiment for **1c** corresponded to the interconversion of enantiomeric conformers of **1c** (e.g., between conformers (i) and (ii), Fig. 4). The main step in this process was proposed to involve the C13–N14 amide passing through the 12-membered ring although flipping of the C5–C6 dicarbonyl unit is also required. Initial attempts to identify a reasonable pathway for the movement of the amide by driving the C14a–N14–C13–O13 torsion angle (amide bond rotation through the ring) in conformer (i) of **1c** were discouraging (see structure in Fig. 1A for numbering). However, progress was made when an initial flip of the C5–C6 dicarbonyl functionality was attempted. This dicarbonyl flip was briefly described in Part 1[4] for the 10-membered ring in **1a** and in the case of **1c** was calculated by driving the O5–C5–C6–O6 torsion angle using the semi-empirical RM1 method and refined at the B3LYP/6-31G** level of theory. The calculations confirmed that conversion of conformer (i) to intermediate conformer (I1) via transition state (TS1) for **1c** (Fig. 4) was an energetically uphill but feasible process, as was the case for **1a**.[4] Importantly, starting at conformer (I1), it was now possible to identify a reasonable path by which the

Table 3
Activation parameters $\Delta G^{\ddagger}_{298}$ [kJ mol^{-1}], $\Delta H^{\ddagger}$ [kJ mol^{-1}] and $\Delta S^{\ddagger}$ [J.K^{-1}.mol^{-1}] for the dynamic process associated with the medium-sized ring in **1a**–**c** were determined experimentally using total lineshape analysis and the intensities of the EXSY crosspeaks between the ^{1}H NMR resonances associated with the C7-diastereotopic protons. Calculated values were generated at the B3LYP/6-31G** level of theory and are given for the corresponding rate determining step (RDS), which varies for each particular analogue (see main text)

	Total lineshape analysis			EXSY			B3LYP/6-31G**			
	$\Delta G^{\ddagger}_{298}$	$\Delta H^{\ddagger}$	$\Delta S^{\ddagger}$	$\Delta G^{\ddagger}_{298}$	$\Delta H^{\ddagger}$	$\Delta S^{\ddagger}$	RDS	$\Delta G^{\ddagger}_{298}$	$\Delta H^{\ddagger}$	$\Delta S^{\ddagger}$
1a	78.4±0.1	76.8±1.7	−5.6±4.9	76.5±0.1	79.8±0.3	11.1±1.0	(i)→(TS1)	72.5	70.6	−7.0
							(I1)→(TS2′)	71.7	66.9	−15.9
1b	80.2±0.4	77.7±4.9	−8.5±13.6	80.5±0.1	78.4±1.2	−7.0±3.6	(I1)→(TS2′)	79.8	73.5	−21.0
1c	58.8±0.1	49.5±0.6	−31.1±2.1	—	—	—	(I1)→(TS2)	61.8	53.9	−26.3

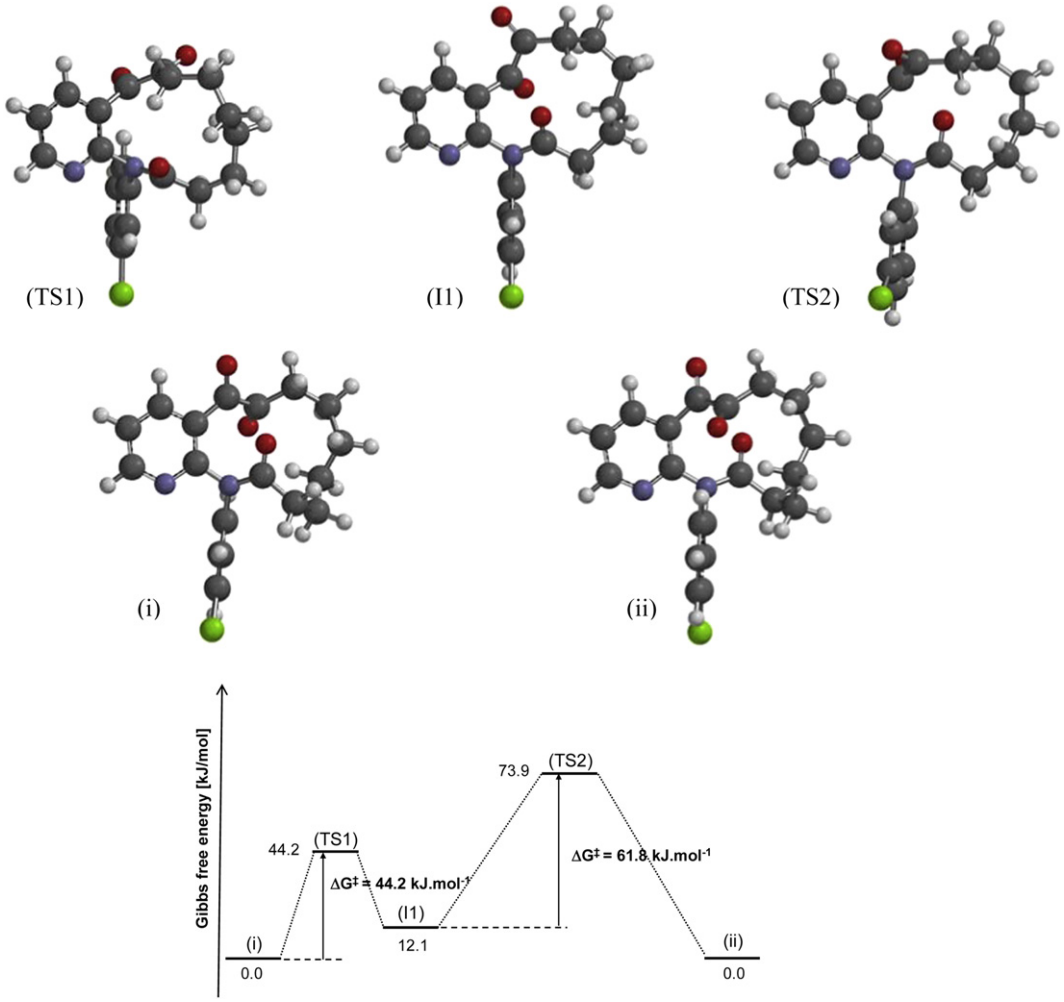

Fig. 4. The fixed amide rotation pathway. Ball and stick representation of ground and transition state structures involved in this pathway for **1c** localised using semi-empirical RM1 method and refined at B3LYP/6-31G** level of theory. The Gibbs free energy profile calculated for this pathway at the same level of theory.

C13–N14 amide could pass through the 12-membered ring by progressive driving of the C4a–C14a–C13–O13 torsion angle from+30° to −70°. The geometry of the transition state (TS2) for this process was refined at the B3LYP/6-31G** level of theory and shows that during this process the C13N14-amide in **1c** travels through the medium-sized ring (the C4a–C14a–C13–O13 torsion angle in (TS2)=−0.9°) without distortion of the amide away from planarity (C14a–N14–C13–O13=−4.7°, Fig. 4). For this reason, this pathway is subsequently referred to as the fixed amide rotation pathway. The calculated Gibbs free energy profile for this overall process is depicted in Fig. 4 and suggests that transition from conformer (I1) to (ii) is the rate determining step for the interconversion of the enantiomeric conformers of **1c**. As the half-life ($t_{1/2}$) for interconversion of (i) to (ii) for **1c** was calculated to be 2.3 ms at 298 K then **1c** does not exist as atropisomers (as defined by Oki[12]). The corresponding activation parameters calculated at the B3LYP/6-31G** level of theory for the fixed amide rotation pathway are in very good agreement with the experimentally determined values (Table 3).

Having rationalised the activation parameters associated with **1c**, an analogous explanation (initial dicarbonyl flip followed by passing of the amide through the medium-sized ring) was computationally assessed for both **1a** and **1b**. As expected, the initially required dicarbonyl flip was energetically feasible for **1b** and **1a** (see Part 1[4]). However, the dicarbonyl flip was calculated to be more difficult as the ring size decreased (the relative Gibbs free energies of both (TS1) and (I1) with respect to the original global minimum ground state (i) are shown as a function of ring size in Table 4) although it is energetically feasible for all three compounds **1a**–**c**.

Table 4
Relative Gibbs free energies of transition states and intermediate conformers with respect to the global minimum ground state (i) calculated at the B3LYP/6-31G** level of theory for analogues **1a**–**c**

	ΔG_{298} [kJ mol]							
	(i)	(TS1)	(I1)	(TS2)	(ii)	(TS2′)	(I2′)	(TS3′)
1a	0.0	72.5	31.0	N/A	0.0	102.7	44.5	101.6
1b	0.0	58.8	24.6	110.1	0.0	104.4	29.8	97.8
1c	0.0	44.2	12.1	73.9	0.0	96.8	31.1	109.1

Next, attempts were made to force the amide group through the 11-membered ring in **1b**. In this case, calculations showed that the fixed amide rotation pathway described for **1c** is plausible for **1b** although there is a significantly higher activation barrier ($\Delta G^{\ddagger}_{298}$=85.5 kJ mol^{-1}, Fig. 6). This value is reasonably consistent with the $\Delta G^{\ddagger}_{298}$ value observed in the VT experiments ($\Delta G^{\ddagger}_{298}$=80.5 kJ mol^{-1}, Table 3, column 5). By contrast, attempts to locate the analogous transition state for the 10-membered ring system **1a** using semi-empirical RM1 methods resulted in unrealistic structures with relative energies above 200 kJ mol^{-1}. As EXSY experiments had clearly shown that the C7-diastereotopic

protons in **1a** could interconvert, an alternative rationalisation to the fixed amide rotation pathway was required for **1a** and possibly **1b**.

*2.5.3. Detailed assessment of **1a**.* As conformer (I1) had proved a more productive starting point in the case of **1c** (Fig. 4), a detailed search of the conformational behaviour of the analogous I1 conformer of **1a** using semi-empirical RM1 method was carried out. Interestingly, it was found that the mirror image of the **1a** ground state geometry could be accessed from conformer (I1) by progressive driving of O11–C11–N12–C1′ dihedral angle from −170° to 170° (see Fig. 1A for numbering). This process can be viewed as a '*trans–cis–trans*' amide bond rotation which flips both the C11N12-amide carbonyl and the *N*12-chlorophenyl ring in **1a**. The amide moiety in both the global minimum ground state (i) and the intermediate conformer (I1) adopts a trans-orientation (O11–C11–N12–C1′=−166.2° and −167.9°, respectively). The transformation is calculated to be achieved through two transition states (TS2′) and (TS3′) and the intermediate conformer (I2′), which has a *cis*-configured amide (O11–C11–N12–C1′=4.8°, Fig. 5). The relative Gibbs free energies with respect to the global minimum ground state (i) obtained after refinement at the B3LYP/6-31G** level of theory are summarised for **1a** in Table 4. The overall Gibbs free energy profile for interconversion of the enantiomeric conformers of **1a** calculated at the B3LYP/6-31G** level of theory shows three activation barriers (Fig. 5). In this process, flipping of the C5–C6 dicarbonyl group also starts the interconversion process as the activation barrier for rotation about the C11–N12 amide bond in conformer (i) is some 30 kJ mol^{-1} higher in energy than that from conformer (I1) for **1a** (data not shown). The calculated Gibbs free energy of activation for the first and second steps in the *trans–cis–trans* amide bond rotation pathway are very close in value ($\Delta G^{\ddagger}_{298}$=72.5 and 71.7 kJ mol^{-1}, respectively) and are significantly larger than for the final step in the pathway ($\Delta G^{\ddagger}_{298}$=57.1 kJ mol^{-1}). Although the similarity in $\Delta G^{\ddagger}_{298}$ for the two steps does not allow for an unambiguous determination of the rate determining step, the $\Delta H^{\ddagger}_{298}$ and $\Delta S^{\ddagger}_{298}$ values calculated for the first step are in better agreement with the experimental values.

*2.5.4. Reassessment of **1c**.* To date two alternative pathways, the fixed amide and the *trans–cis–trans amide bond* rotation pathways, have been identified by which enantiomeric conformers in this series can interconvert. The most clear situation is for the 10-membered ring containing **1a**, where the only energetically feasible pathway is the *trans–cis–trans amide bond* rotation pathway described in Fig. 5. Reanalysis of **1c** showed that this pathway was also feasible for **1c** (see Table 4) but that the activation barriers for this pathway are significantly higher for **1c** than those calculated for the fixed amide rotation pathway (Fig. 4). It was therefore concluded that, whilst both **1a** and **1c** are both capable of interconverting enantiomeric conformers, they do so by different pathways. Next the focus turned to **1b**, which contains an 11-membered ring intermediate in size between the rings in **1a** and **1c**.

*2.5.5. Detailed assessment of **1b**.* Conformational intermediates and transition states for both amide rotation pathways were calculated for **1b**. The resulting relative energies with respect to the corresponding global minimum ground state (i) are summarised in Table 4 and are depicted in Fig. 6. Unlike the situation for transition state (TS1) and conformational intermediate (I1), the relative energies of both the transition states (TS2′) and (TS3′) are only slightly affected by the ring size (Table 4). Consequently the Gibbs free

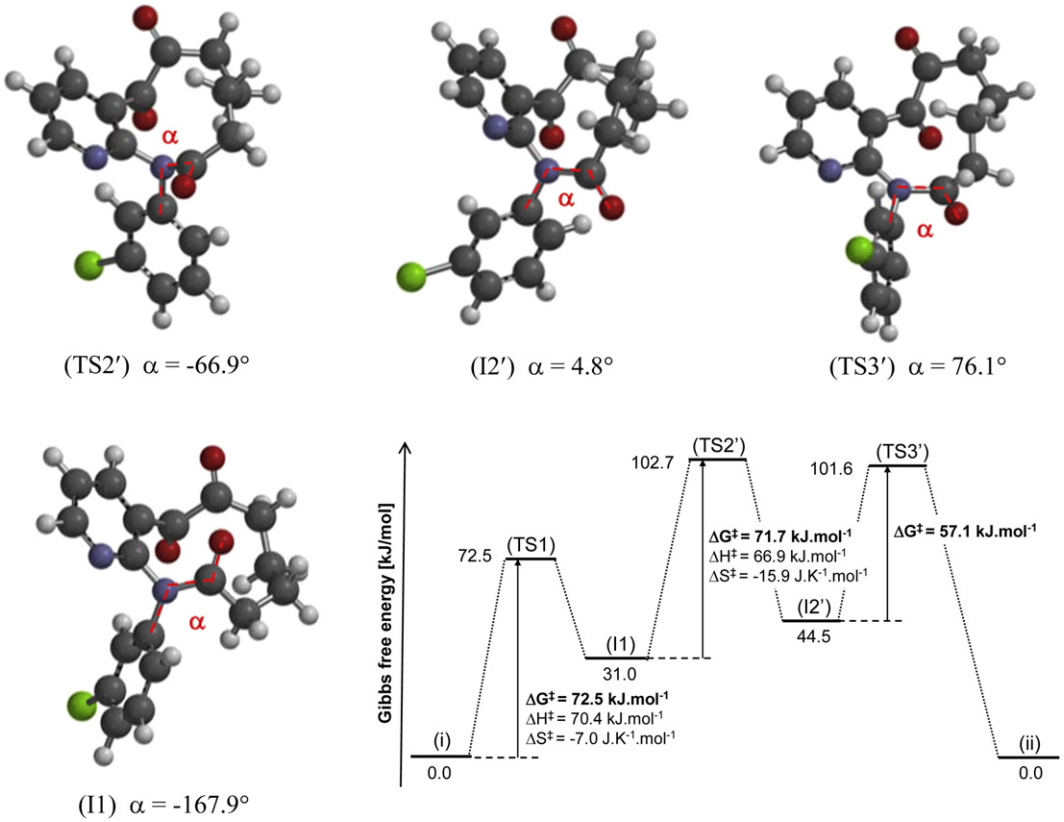

Fig. 5. *trans–cis–trans* amide bond rotation pathway: Ball and stick representation of ground and transition state structures for amide rotation of **1a** localised using semi-empirical RM1 method and refined at the B3LYP/6-31G** level of theory. The key torsion angle α=O11–C11–N12–C1′ is highlighted by red dashed line. The free energy profile for interconversion of mirror images of **1a** calculated at the B3LYP/6-31G** level of theory is also shown.

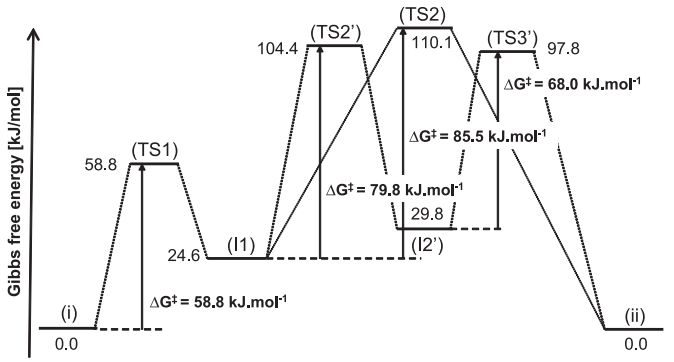

Fig. 6. Gibbs free energy profile for the interconversion of the mirror images of **1b** calculated at the B3LYP/6-31G** level of theory.

energy for the transition from (I1) to (TS2′) becomes larger for **1b** compared to the situation for **1a** but the calculated barrier for **1b** is still smaller than the barrier calculated for the fixed amide rotation pathway via transition state (TS2) for **1b** (Fig. 6). Thus the most favoured pathway for **1b** is calculated to be the *trans–cis–trans amide bond* rotation pathway seen for **1a**, although a key difference exist as the rate determining step is clearly the conversion of (I1) to (I2′) for **1b**. Gratifyingly, the experimental and calculated values of the activation parameters associated with **1b** (Table 3), assuming that the process observed in the VT NMR experiments is the conversion of (I1) to (I2′), are in good agreement.

3. Conclusion

The attempted synthesis of the 10-membered ring containing **1a** from **2a** led to a compound that exhibited a relatively complex ^{1}H NMR at room temperature. In addition, X-ray crystallographic analysis of **1a** showed that two enantiomeric pairs of conformers were present in the unit cell. These observations raised the possibility that **1a** existed as enantiomeric atropisomers, which in theory could be isolated. It was initially proposed that this might result from the fact that the amide carbonyl group in **1a** was unable to pass through the 10-membered ring, hence rendering interconversion of enantiomeric conformers of **1a** impossible. This naive view led to a proposal that investigation of the ring-expanded versions of **1a**, compounds **1b** (11-membered ring) and **1c** (12-membered ring) may cast further light on the system. Indeed it was found through variable temperature NMR studies using **1c** that interconversion of the enantiomeric conformers of **1c** was relatively fast with a $t_{1/2}$ for this process of approximately 2 ms. Furthermore it was shown by computational methods that the interconversion of enantiomeric conformers of **1c** very likely occurred by passage of the amide bond in **1c** through the 12-membered ring, oreceded by a C5–C6 dicarbonyl flip. As the calculations suggest that the amide bond in **1c** remains in a *trans*-orientation throughout this process it has been referred to here as the fixed amide rotation pathway. Intriguingly, when the analogous process was explored computationally for **1a** it was shown that the fixed amide rotation pathway was impossible in the 10-membered ring series.

Further light was cast on the 10-membered system **1a** when a 1D gs-NOESY/EXSY experiment demonstrated that interconversion of the diastereotopic protons in **1a** was occurring on the NMR timescale. This observation was also consistent with the half-life calculated from the activation parameters determined for **1a** using VT NMR techniques ($t_{1/2}$ (**1a**)=4.3 s at 298 K). Whilst this information argues that **1a** cannot exists as atropisomers (as defined by Oki[12]), the question of how the enantiomeric conformers of **1a** interconvert remained. Further computational studies led to the identification of a pathway that could explain this observation provided the amide bond in **1a** undergoes *trans*- to *cis*- to *trans*-isomerisation after a flip of the C5–C6 dicarbonyl group has occurred. By this pathway (the *trans–cis–trans amide bond rotation pathway*), which was shown to be energetically feasible for **1a**, the two enantiomeric conformers of **1a** can interconvert without the amide group passing through the 10-membered ring. Whilst **1a** and **1c** use two different pathways to interconvert enantiomeric conformers, the situation for the 11-membered ring containing analogue **11b** is less certain as both processes are calculated to be energetically feasible. Our current studies suggest that **11b** preferentially uses the *trans–cis–trans amide bond rotation pathway*.

A combination of synthesis, NMR and computational methods has led to an improved understanding of the conformational equilibria associated with a set of medium-sized ring containing analogues. Future reports will focus on the study of related systems where interconversion of enantiomeric conformers is not possible.

4. Experimental[11]

4.1. General procedure A[8]

A solution of triethylamine (4.81 mL, 34.5 mmol, 1.10 equiv) and the enamine (**3a** (13.6 g, 34.5 mmol, 1.10 equiv) or **3b** (14.9 g, 34.5 mmol, 1.10 equiv) or **3c** (16.1 g, 34.5 mmol, 1.10 equiv)) in toluene (18.0 mL) was added dropwise over 10 min to a stirred, cooled (ice–acetone, −10 °C bath) suspension of crude 2-((3-chlorophenyl) amino)-3-pyridinecarbonyl chloride (8.40 g, 31.4 mmol, 1.00 equiv) in toluene (140 mL). As the solid dissolved, the dark red reaction mixture was kept between −5 °C and +5 °C for 2 h, then allowed to warm up to room temperature over 30 min and heated at 80 °C for 4 h. After cooling down, the reaction mixture was stirred at room temperature for 12 h, after which the toluene was removed under reduced pressure. The residue was dissolved in dichloromethane (150 mL) and the solution was washed with H_2O (100 mL), 1.0 M $HCl_{(aq)}$ (100 mL), 1.0 M $Na_2CO_{3(aq)}$ (100 mL) and with H_2O (100 mL). Aqueous extracts were back extracted with dichloromethane (2×150 mL), and the combined organic portion was dried over Na_2SO_4, filtered and concentrated in vacuo. The residue was purified by column chromatography over silica gel (3:2, ethyl acetate/hexane). An analytically pure sample was obtained by recrystallisation from acetonitrile to afford the title compound.

4.2. General procedure B

To a solution of **2** (**2a** (311 mg, 1.00 mmol, 1.00 equiv) or **2b** (325 mg, 1.00 mmol, 1.00 equiv) or **2c** (339 mg, 1.00 mmol, 1.00 equiv)) in anhydrous dichloromethane (16.0 mL) was added portion-wise *m*-CPBA (345 mg, 2.00 mmol, 2.00 equiv) and the reaction mixture was stirred at room temperature for 40 h before being washed with 1.0 M $Na_2CO_{3(aq)}$ (10.0 mL) and H_2O (10.0 mL). The aqueous washes were back extracted with dichloromethane (2×30.0 mL). The combined organic layers were dried ($MgSO_4$), filtered and concentrated in vacuo. The residue was purified by column chromatography over silica gel (1:1, ethyl acetate/hexane). An analytically pure sample was obtained by recrystallisation from ethanol.

4.3. General procedure C

A solution of the cyclic ketone (cycloheptanone **4b** (10.1 g, 90.0 mmol, 1.00 equiv) or cyclooctanone **4c** (11.4 g, 90.0 mmol, 1.00 equiv)), pyrrolidine (8.26 mL, 99.0 mmol, 1.10 equiv) and *p*-toluenesulfonic acid (catalytic 0.01 g) in anhydrous toluene (200 mL) was refluxed under argon using a Dean and Stark apparatus. Refluxing whilst stirring was continued until separation of water had ceased (**3b**, 5 h and **3c**, 20 h). The reaction mixture was

then cooled and the solution concentrated in vacuo. The residue was purified by distillation.

*4.3.1. 13-(3-Chlorophenyl)-8,9,10,11-tetrahydro-5H-pyrido[2,3-b][1] azacycloundecine-5,6,12-(7H,13H)-trione (**1b**).* The title compound **1b** (257 mg, 0.720 mmol, 72%) was afforded as a yellow solid using general procedure B.

Mp 115–116 °C; ^{1}H NMR (300 MHz, $CDCl_3$): δ=8.29 (dd, ^3J=4.9 Hz, ^4J=2.0 Hz, 1H, C2-*H*), 8.04 (dd, ^3J=7.7 Hz, ^4J=2.0 Hz, 1H, C4-*H*), 7.34–7.30 (m, 1H, Ar–*H*), 7.29–7.23 (m, 2H, Ar–*H*), 7.22–7.17 (m, 1H, Ar–*H*), 7.14–7.09 (m, 1H, C3-*H*), 3.44–3.30 (m, 1H, C7-*H*), 2.65–2.54 (m, 1H, C7′-*H*), 2.34–2.21 (m, 1H, C11-*H*), 2.07–1.98 (m, 1H, C11′-*H*), 1.92–1.78 (m, 1H, C8-*H*), 1.69–1.46 (m, 4H, C8′-*H*, C10-H_2, C9-*H*), 1.22–1.08 (m, 1H, C9′-*H*); ^{13}C NMR (75.5 MHz, $CDCl_3$): δ=201.5 (C6), 188.8 (C5), 175.5 (C12), 151.6 (C2), 151.4 (C13a), 142.6 (C1′), 139.2 (C4), 135.1 (C3′), 130.5 (Ar), 129.9 (Ar), 128.8 (Ar), 128.0 (Ar), 126.0 (C4a), 121.8 (C3), 36.0 (C11), 34.3 (C7), 25.0 (C9), 22.5 (C10), 21.5 (C8); IR (KBr): ν_{max} 2944 (m), 1710 (s) (C=O), 1686 (s) (C=O), 1655 (s) (C=O), 1589 (s), 1475 (m), 1423 (m), 1364 (m), 1266 (s), 741 (s) cm^{-1}; LRMS (ES$^+$): *m*/*z* (%) 379.18 (100) [M^{35}Cl+Na]$^+$; HRMS (ES$^+$): *m*/*z* calcd for $C_{19}H_{17}^{35}ClN_2NaO_3$ [M^{35}Cl+Na]$^+$: 379.0835; found: 379.0825.

*4.3.2. 14-(3-Chlorophenyl)-7,8,9,10,11,12-hexahydropyrido[2,3-b][1] azacyclododecine-5,6,13-(14H)-trione (**1c**). Method* 1: The title compound **1c** (89 mg, 0.24 mmol, 24%) was afforded as a yellow oil using general procedure B with an additional 20 h stirring at room temperature. ^{1}H NMR (300 MHz, $CDCl_3$): δ=8.41 (dd, ^3J=4.8 Hz, ^4J=2.0 Hz, 1H, C2-*H*), 8.01 (dd, ^3J=7.7 Hz, ^4J=2.0 Hz, 1H, C4-*H*), 7.57–7.53 (m, 1H, Ar–*H*), 7.46–7.41 (m, 3H, Ar–*H*), 7.23 (dd, ^3J=7.7, 4.8 Hz, 1H, C3-*H*), 3.96–3.41 (m, 1H, C7-*H*), 2.53–1.39 (m, 11H, C7′-*H*, C12-H_2, C8-H_2, C9-H_2, C11-H_2, C10-H_2); ^{13}C NMR (75.5 MHz, $CDCl_3$): δ=199.6 (C6), 187.8 (C5), 173.7 (C13), 150.8 (C14a), 150.5 (C2), 142.0 (C1′), 139.2 (C4), 135.0 (C3′), 130.4–129.0 (4×Ar), 126.5 (C4a), 121.6 (C3), 34.2 (C12), 26.0 (C7), 24.8 (C9), 24.5 (C10), 23.3 (C11), 21.2 (C8); IR (NaCl): ν_{max}=2932 (m), 1693 (s) (C=O), 1665 (s) (C=O), 1591 (s), 1475 (w), 1420 (m), 1368 (m), 1274 (m) cm^{-1}; LRMS (ES$^+$): *m*/*z* (%) 393.19 (100) [M^{35}Cl+Na]$^+$; HRMS (ES$^+$): *m*/*z* calcd for $C_{20}H_{19}^{35}ClN_2NaO_3$ [M^{35}Cl+Na]$^+$: 393.0982; found: 393.0967.

When 4.0 equiv of *m*-CPBA was used, **1c** was obtained as a yellow oil (133 mg, 0.360 mmol, 36%). In addition, aldehyde **5** (116 mg, 0.300 mmol, 30%) and **2c** (115 mg) were isolated from this reaction.

Method 2: A. Sodium periodate (321 mg, 1.50 mmol, 3.00 equiv) was stirred in H_2O (0.750 mL) and 2 N sulfuric acid (100 μL, 0.100 mmol, 20 mol %). After the solid had dissolved, the solution was cooled to 0 °C. Ruthenium(III) chloride hydrate (519 μg, 0.00300 mmol, 0.5 mol %) was then added and the reaction was stirred until the colour turned bright yellow. Ethyl acetate (3 mL) and acetonitrile (3 mL) were added and stirring was continued for a further 5 min **2c** (169 mg, 0.500 mmol, 1.00 equiv) was then added to the reaction and the slurry was stirred at room temperature for 24 h. The reaction mixture was poured into a mixture of saturated $NaHCO_3$ solution (10.0 mL) and saturated sodium thiosulfate solution (10.0 mL). The phases were separated, and the aqueous layer was extracted with ethyl acetate (3×20.0 mL). The combined organic layers were dried (Na_2SO_4) and concentrated in vacuo. The crude product was purified by flash column chromatography using silica gel (4:6, ethyl acetate/hexane) to afford **1c** (30.0 mg, 0.0800 mmol, 16%) as a white solid; B. Method 2A was repeated using ruthenium(III) chloride hydrate (5.19 mg, 0.0300 mmol, 5.0 mol %) to afford **1c** (69.0 mg, 0.190 mmol, 37%) as a white solid.

*4.3.3. 11-(3-Chlorophenyl)-6,7,8,9,10,11-hexahydro-5H-cyclohepta [b][1,8]naphthyridin-5-one (**2b**).* The title compound **2b** (4.08 g, 12.6 mmol, 40%) was afforded as a cream solid using general procedure A. Mp 168–169 °C; ^{1}H NMR (300 MHz, $CDCl_3$): δ=8.73 (dd, ^3J=7.9 Hz, ^4J=2.0 Hz, 1H, C4-*H*), 8.51 (dd, ^3J=4.5 Hz, ^4J=2.0 Hz, 1H, C2-*H*), 7.53–7.50 (m, 2H, Ar–*H*), 7.28–7.24 (m, 2H, Ar–*H*, C3-*H*), 7.17–7.13 (m, 1H, Ar–*H*), 3.08–2.93 (m, 2H, C6-H_2), 2.64–2.59 (m, 2H, C10-H_2), 1.87–1.79 (m, 2H, C8-H_2), 1.67–1.60 (m, 2H, C7-H_2), 1.59–1.52 (m, 2H, C9-H_2); ^{13}C NMR (75.5 MHz, $CDCl_3$): δ=176.5 (C5), 155.4 (C10a), 151.9 (C2), 151.1 (C11a), 140.8 (C1′), 136.1 (C4), 135.3 (C3′), 130.7 (Ar), 129.8 (Ar), 129.4 (Ar), 127.7 (Ar), 124.9 (C5a), 119.6 (C3), 119.3 (C4a), 32.2 (C10), 32.0 (C8), 26.7 (C7), 25.5 (C9), 24.1 (C6); IR (KBr): ν_{max}=2932 (m), 1617 (s) (C=O), 1589 (m), 1542 (w), 1475 (m), 1425 (m), 1296 (m), 785 (m), 750 (w) cm^{-1}; LRMS (ES$^+$): *m*/*z* (%) 347.13 (100) [M^{35}Cl+Na]$^+$; HRMS (ES$^+$): *m*/*z* calcd for $C_{19}H_{17}^{35}ClN_2NaO$ [M^{35}Cl+Na]$^+$: 347.0927; found: 347.0913.

*4.3.4. 12-(3-Chlorophenyl)-6,7,8,9,10,11-hexahydrocycloocta[b][1,8] naphthyridin-5(12H)-one (**2c**).* The title compound **2c** (5.43 g, 16.0 mmol, 51%) was afforded as a cream solid using general procedure A. Mp 190–191 °C; ^{1}H NMR (300 MHz, $CDCl_3$): δ=8.74 (dd, ^3J=7.6 Hz, ^4J=1.9 Hz, 1H, C4-*H*), 8.51 (dd, ^3J=4.6 Hz, ^4J=1.9 Hz, 1H, C2-*H*), 7.55–7.50 (m, 2H, Ar–*H*), 7.31–7.25 (m, 2H, Ar–*H*, C3-*H*), 7.21–7.18 (m, 1H, Ar–*H*), 2.96–2.83 (m, 2H, C6-H_2), 2.74–2.69 (m, 2H, C11-H_2), 1.81–1.73 (m, 2H, C7-H_2), 1.56–1.42 (m, 6H, C10-H_2, C8-H_2, C9-H_2); ^{13}C NMR (75.5 MHz, $CDCl_3$): δ=177.0 (C5), 151.9 (C2), 151.7 (C12a), 151.6 (C11a), 140.6 (C1′), 136.0 (C4), 135.3 (C3′), 130.5 (Ar), 130.1 (Ar), 129.6 (Ar), 128.1 (Ar), 123.4 (C5a), 119.5 (C3), 119.2 (C4a), 29.6 (C8), 29.5 (C7), 29.2 (C11), 27.6 (C10), 25.7 (C9), 25.2 (C6); IR (KBr): ν_{max}=1617 (s) (C=O), 1588 (m), 1543 (m), 1475 (m), 1426 (m), 1266 (s), 745 (s) cm^{-1}; LRMS (ES$^+$): *m*/*z* (%) 361.11 (100) [M^{35}Cl+Na]$^+$, 699.27 (25) [2M^{35}Cl+Na]$^+$, 363.15 (10) [[M^{37}Cl+Na]$^+$, 701.28 (10) [M^{35}Cl+M^{37}Cl+Na]$^+$; HRMS (ES$^+$): *m*/*z* calcd for $C_{20}H_{20}^{35}ClN_2O$ [M^{35}Cl+H]$^+$: 339.1264; found: 339.1268.

*4.3.5. (E)-1-Cycloheptenylpyrrolidine[13] (**3b**).* The title compound **3b** (9.20 g, 55.7 mmol, 62%) was afforded as a yellow oil after distillation using general procedure C. ^{1}H NMR (300 MHz, $CDCl_3$): δ=4.47 (br s, 1H, C2-*H*), 2.97–2.91 (m, 4H, C2′-H_2), 2.49–2.45 (m, 4H, C3-H_2, C7-H_2), 1.84–1.80 (m, 4H, C3′-H_2), 1.73–1.62 (m, 6H, C4-H_2, C6-H_2, C5-H_2); LRMS (ES$^+$): *m*/*z* (%) 166.15 (100) [M+H]$^+$.

*4.3.6. (E)-1-Cyclooctenylpyrrolidine[13] (**3c**).* The title compound **3c** (13.9 g, 77.5 mmol, 86%) was afforded as a yellow oil after distillation using general procedure C. ^{1}H NMR (300 MHz, $CDCl_3$): δ=4.27 (br s, 1H, C2-*H*), 3.15–3.08 (m, 4H, C2′-H_2), 2.52–2.43 (m, 4H, C3-H_2, C8-H_2), 2.28–2.17 (m, 2H, C4-H_2), 2.01–1.91 (m, 4H, C3′-H_2), 1.68–1.54 (m, 6H, C5-H_2, C7-H_2, C6-H_2); LRMS (ES$^+$): *m*/*z* (%) 180.12 (100) [M+H]$^+$.

*4.3.7. 6-(1-(3-Chlorophenyl)-3-hydroxy-2,4-dioxo-1,2,3,4-tetrahydro-1,8-naphthyridin-3-yl)-hexanal (**5**).* The title compound **5** (116 mg, 0.300 mmol, 30%) was afforded as a yellow solid using general procedure B with an additional 20 h stirring at room temperature.

Mp 93–94 °C; ^{1}H NMR (400 MHz, $CDCl_3$): δ=9.73 (t, ^3J=1.4 Hz, 1H, C12-H), 8.47 (dd, ^3J=4.8 Hz, ^4J=1.9 Hz, 1H, C2-*H*), 8.29 (dd, ^3J=7.6 Hz, ^4J=1.9 Hz, 1H, C4-*H*), 7.48–7.47 (m, 2H, C5′-*H* and C4′-*H*), 7.22–7.18 (m, 2H, C6′-*H* and C3-*H*), 7.11 (br s, 1H, C2′-*H*), 2.41 (td, ^3J=7.2 Hz, ^4J=1.4 Hz, 1H, C11-*H*), 2.09–1.94 (m, 2H, C7-*H*), 1.64–1.56 (m, 2H, C10-H_2), 1.54–1.40 (m, 2H, C8-H_2), 1.35–1.24 (m, 2H, C9-H_2); ^{13}C NMR (100.6 MHz, $CDCl_3$): δ=202.5 (C12), 193.6 (C5), 173.1 (C13), 154.8 (C2), 154.4 (C1a), 137.4 (C1′), 137.2 (C4), 135.5 (C3′), 130.9 (C5′), 129.7 (C4′ and C3), 127.5 (C2′), 120.3 (C6′), 115.8 (C4a), 83.4 (C6), 43.9 (C11), 41.1 (C7), 29.0 (C10), 23.1 (C8), 22.0 (C11); IR (NaCl): ν_{max}=3409 (OH), 2926 (m), 1722 (s) (C=O), 1688 (s) (C=O), 1587 (s), 1469 (w), 1435 (m), 1346 (m), 1174 (C–N), 773 (s), 732 (s) cm^{-1}; LRMS (ES$^+$): *m*/*z* (%) 408.8 (100) [M^{35}Cl+Na]$^+$, 440.8 (30)

[$M^{35}Cl$+Na+MeOH]; HRMS (ES^+): *m*/*z* calcd for $C_{20}H^{35}_{19}ClN_2NaO_3$ [$M^{35}Cl$+Na]$^+$: 409.0931; found: 409.0942.

4.4. Computational methods

Semi-empirical electronic structure calculations were carried out using the RM1 method[14] as implemented in Spartan '08 (Version 1.1.2, Build 131)[15] running on Windows XP computer equipped with a Intel Core 2 Quad processor at 2.67 GHz and 4 GB of memory. DFT calculations were carried using the same software and hardware. The transition states were located by generation of an initial guess using the results of the RM1 calculations. This model transition state was refined at the B3LYP/6-31G** level of theory to a transition state structure possessing single imaginary vibration that corresponded to the coordinate under study.

4.5. Dynamic NMR spectroscopy

All dynamic NMR experiments were carried out using a Bruker AVANCE 500 spectrometer equipped with inverse tuneable BBI probe. The temperature, controlled by a Bruker BVT unit, was measured before each experiment using either 4% MeOH in methanol-d_4 or 80% 1,2-ethanediol in DMSO-d_6 samples.[16] The rate constants for exchange processes were determined by complete lineshape analysis using the Bruker TOPSPIN DNMR module and/or quantitative EXSY experiment.[17] 1D NOESY/EXSY experiments were recorded using standard *selnogp* sequence with 50 ms 180° Gaussian pulse for selective inversion of H7 resonances and mixing times ranging from 0 to 0.4 s.[18] The resultant intensities of EXSY crosspeaks were heightened by the addition of NOE crosspeaks intensities obtained from the same experiment recorded at room temperature and these were evaluated using EXSYCalc software (Mestrelab Research). The temperature dependence of rate constants was used to determine the activation parameters by fitting the experimental data to the Eyring equation.

Acknowledgements

The authors thank BBSRC (A.M.J.), the Wellcome Trust (M.M.L.) and the Royal Society (Research Fellowship to N.J.W.) for funding.

Supplementary data

Supplementary data associated with this article can be found in online version at doi:10.1016/j.tet.2010.10.043.

References and notes

1. (a) Dolle, R. E.; Le Bourdonnec, B.; Goodman, A. J.; Morales, G. A.; Thomas, C. J.; Zhang, W. *J. Comb. Chem.* **2009**, *11*, 739–790 and previous articles in this review series; (b) Kim, Y.; Arai, M. A.; Arai, T.; Lamenzo, J. O.; Dean, E. F., III; Patterson, N.; Clemons, P. A.; Schreiber, S. L. *J. Am. Chem. Soc.* **2004**, *126*, 14740–14745.
2. For a brief discussion see Wessjohann, L. A.; Rivera, D. G.; Vercillo, O. E. *Chem. Rev.* **2009**, *109*, 796–814.
3. For some recent examples of library synthesis involving medium-sized rings see: (a) Lee, D.; Sello, J. K.; Schreiber, S. L. *J. Am. Chem. Soc.* **1999**, *121*, 10648–10649; (b) Spring, D. R.; Krishnan, S.; Blackwell, H. E.; Schreiber, S. L. *J. Am. Chem. Soc.* **2002**, *124*, 1354–1363; (c) Looper, R. E.; Pizzirani, D.; Schreiber, S. L. *Org. Lett.* **2006**, *8*, 2063–2066; (d) Morton, D.; Leach, S.; Cordier, C.; Warriner, S.; Nelson, A. *Angew. Chem., Int. Ed.* **2009**, *48*, 104–109.
4. Jones, A.M.; Lorion, M.M.; Lebl, T.; Slawin, A.M.Z.; Philp, D.; Westwood, N.J. *Tetrahedron*, 2010.
5. Friary, R. J.; Schwerdt, J. H. *Tetrahedron* **1991**, *47*, 9981–9984.
6. Crystallographic data (excluding structure factors) for **1a** has been deposited with the Cambridge Crystallographic Data Centre as supplementary publication no. CCDC 741362. Copies of the data can be obtained, free of charge, on application to CCDC, 12 Union Road, Cambridge CB2 1EZ, UK, (fax: +44(0)1223 336033 or e-mail: deposit@ccdc.cam.ac.uk/).
7. For some recent example of atropisomerism in medium-sized rings see: (a) Gibson, K. R.; Hitzel, L.; Mortshire-Smith, R. J.; Gerhard, U.; Jelley, R. A.; Reeve, A. J.; Rowley, M.; Nadin, A.; Owens, A. P. *J. Org. Chem.* **2002**, *67*, 9354–9360; (b) Lee, S.; Kamide, T.; Tababta, H.; Takahashi, H.; Shiro, M.; Natsugari, H. *Biorg. Med. Chem.* **2008**, *16*, 9519–9523; (c) King, F. D.; Aliev, A. E.; Caddick, S.; Tocher, D. A.; Coutier-Murias, D. *Org. Biomol. Chem.* **2009**, *7*, 167–177.
8. (a) Friary, R. J.; Seidl, V.; Schwerdt, J. H.; Chan, T.-M.; Cohen, M. P.; Conklin, E. R.; Duelfer, T.; Hou, D.; Nafissi, M.; Runkle, R. L.; Tahbaz, P.; Tiberi, R. L.; McPhail, A. T. *Tetrahedron* **1993**, *49*, 7179–7192; (b) Friary, R. J.; Seidl, V.; Schwerdt, J. H.; Cohen, M. P.; Hou, D.; Nafissi, M. *Tetrahedron* **1993**, *49*, 7169–7178.
9. (a) Davies, S. G.; Key, M.-S.; Rodriquez-Solla, H.; Sanganee, H. J.; Savory, E. D.; Smith, A. D. *Synlett* **2003**, 1659–1662; (b) Aciro, A.; Davies, S. G.; Garner, A. C.; Ishii, Y.; Key, M.-S.; Ling, K. B.; Prasad, R. S.; Roberts, P. M.; Rodriquez-Solla, H.; O'Leary-Steele, C.; Russell, A. J.; Sanganee, H. J.; Savory, E. D.; Smith, A. D.; Thomson, J. E. *Tetrahedron* **2008**, *64*, 9320–9344.
10. Frunzke, J.; Loschen, C.; Frenking, G. *J. Am. Chem. Soc.* **2004**, *126*, 3642–3652.
11. For a more information see Supplementary data.
12. Oki, M. *Recent Advances in Atropisomerism*, 1st ed.; John Wiley: New York, NY, 1983.
13. Kuehne, M. E. *J. Am. Chem. Soc.* **1959**, *81*, 5400–5404.
14. Rocha, G. B.; Freire, R. O.; Simas, A. M.; Stewart, J. J. P. J. *Comput. Chem.* **2006**, *27*, 1101–1111.
15. Shao, Y.; Molnar, L. F.; Jung, Y.; Kussmann, J.; Ochsenfeld, C.; Brown, S. T.; Gilbert, A. T. B.; Slipchenko, L. V.; Levchenko, S. V.; O'Neill, D. P.; DiStasio, R. A., Jr.; Lochan, R. C.; Wang, T.; Beran, G. J. O.; Besley, N. A.; Herbert, J. M.; Lin, C. Y.; Van Voorhis, T.; Chien, S. H.; Sodt, A.; Steele, R. P.; Rassolov, V. A.; Maslen, P. E.; Korambath, P. P.; Adamson, R. D.; Austin, B.; Baker, J.; Byrd, E. F. C.; Dachsel, H.; Doerksen, R. J.; Dreuw, A.; Dunietz, B. D.; Dutoi, A. D.; Furlani, T. R.; Gwaltney, S. R.; Heyden, A.; Hirata, S.; Hsu, C.-P.; Kedziora, G.; Khalliulin, R. Z.; Klunzinger, P.; Lee, A. M.; Lee, M. S.; Liang, W. Z.; Lotan, I.; Nair, N.; Peters, B.; Proynov, E. I.; Pieniazek, P. A.; Rhee, Y. M.; Ritchie, J.; Rosta, E.; Sherrill, C. D.; Simmonett, A. C.; Subotnik, J. E.; Woodcock, H. L., III; Zhang, W.; Bell, A. T.; Chakraborty, A. K.; Chipman, D. M.; Keil, F. J.; Warshel, A.; Hehre, W. J.; Schaefer, H. F.; Kong, J.; Krylov, A. I.; Gill, P. M. W.; Head-Gordon, M. *Phys. Chem. Chem. Phys.* **2006**, *8*, 3172–3191.
16. Berger, S.; Braun, S. *200 and More NMR Experiments*; Wiley-VCH: Weinheim, 2004.
17. Perrin, C. L.; Dwyer, T. J. *Chem. Rev.* **1990**, *90*, 935–967.
18. Stonehouse, J.; Adell, P.; Keeler, J.; Shaka, A. J. *J. Am. Chem. Soc.* **1994**, *116*, 6037–6038.